ACS Catalysis

Research Article

pubs.acs.org/acscatalysis

Two Different Roles of Metallic Ag on Ag/AgX/BiOX (X = Cl, Br) Visible Light Photocatalysts: Surface Plasmon Resonance and Z-Scheme Bridge

Liqun Ye, Jinyan Liu, Chuqing Gong, Lihong Tian, Tianyou Peng, and Ling Zan*

College of Chemistry and Molecular Science, Wuhan University, Wuhan 430072, People's Republic of China

Supporting Information

ABSTRACT: Ag/AgX/BiOX (X = Cl, Br) three-component visible-light-driven (VLD) photocatalysts were synthesized by a low-temperature chemical bath method and characterized by X-ray diffraction patterns, X-ray photoelectron spectroscopy, field emission scanning electron microscopy, transmission electron microscopy, high-resolution transmission electron microscopy, and UV−vis diffuse reflectance spectra. The Ag/AgX/BiOX composites showed enhanced VLD photocatalytic activity for the degradation of rhodamine B, which was much higher than Ag/AgX and BiOX. The photocatalytic mechanisms were analyzed by active species trapping and superoxide radical quantification experiments. It revealed that metallic Ag played a different role for Ag/AgX/BiOX VLD photocatalysts, surface plasmon resonance for Ag/AgCl/BiOCl, and the Z-scheme bridge for Ag/AgBr/BiOBr.

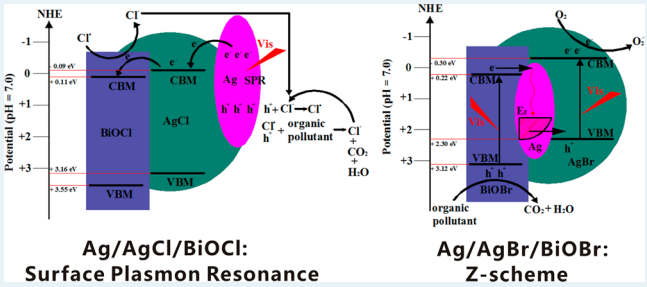

KEYWORDS: *Ag, AgX, BiOX, SPR, Z-scheme*

1. INTRODUCTION

With urbanization and industrialization, the environmental pollution caused by hazardous wastes and toxic air contaminants had been become an overwhelming problem all over the world.[1,2] Semiconductor photocatalysis technique provides a "green" method for completely eliminating most kinds of contaminants, especially some azo dyes.[3] Among the plentiful semiconductor materials, semiconductor TiO_2 has undoubtedly proven to be an excellent photocatalyst for the photocatalytic degradation (PCD) of pollutants in water and air. Unfortunately, TiO_2 displayed low quantum yields and lacked visible light utilization due to its wide band gap of 3.2 eV. Therefore, the development of visible-light-driven (VLD) photocatalysts has attracted great interest.[4]

To date, there are two main synthesis strategies that have been investigated for the preparation of VLD photocatalysts. The first one is to extend the photoresponse of TiO_2 to the visible region by doping, coupling, and sensitization. The other strategy is exploiting novel VLD photocatalysts, such as simple oxides, sulfides, and complex oxides. In recent years, much interest has been paid to designing Ag/AgX (X = Cl, Br, I) composite materials due to the surface plasmon resonance (SPR) of metallic Ag.[5−11] SPR is the resonant photon-induced collective oscillation of valence electrons. It can occur when the frequency of exciting light matches the natural frequency of surface electrons oscillating to resist the restoring force of positive nuclei,[12] so SPR can dramatically enhance the absorption of visible light and provide new opportunities for developing VLD photocatalysts. For example, it has been demonstrated that Ag/AgBr/TiO_2,[4,13−15] Ag/AgBr/Bi_2WO_6,[3] and Ag/AgBr/WO_3[16] show an enhanced VLD photocatalytic activities.

Recently, BiOX (X = Cl, Br) were proved to have very high photocatalytic activities for PCD of azo dyes.[17−21] Furthermore, in our previous research, black BiOCl showed more than 100 times higher photocatalytic activity than P25 TiO_2 under visible light irradiation.[22] To enhance their photocatalytic activities further, we chose Ag/AgCl and Ag/AgBr to couple with BiOCl and BiOBr, respectively. X-ray photoelectron spectroscopy (XPS) and high-resolution transmission electron microscopy (HRTEM) proved the coupling among Ag, AgX, and BiOX (X = Cl, Br). As-synthesized Ag/AgCl/BiOCl and Ag/AgBr/BiOBr samples displayed 59 and 11 times higher photocatalytic activities than BiOCl and BiOBr, respectively. The degradation mechanisms of RhB over the Ag/AgX/BiOX are discussed. It was found that metallic Ag plays a different role in Ag/AgX/BiOX three-component VLD photocatalysts, SPR for Ag/AgCl/BiOCl, and the Z-scheme bridge for Ag/AgBr/BiOBr.

2. EXPERIMENTAL SECTION

2.1. Materials. $Bi(NO_3)_3{\cdot}5H_2O$, $AgNO_3$, *p*-benzoquinone (BQ), isopropyl alcohol (IPA), triethanolamine (TEOA), nitroblue tetrazolium (NBT), cetyltrimethylammonium chlor-

Received: March 29, 2012
Revised: June 13, 2012
Published: July 3, 2012

 © 2012 American Chemical Society

ide (CTAC), cetyltrimethylammonium bromide (CTAB), and ethanol were analytically pure and from Sinopharm Chemical Reagent Co., Ltd. Rhodamine B (RhB) was analytically pure and used without further purification.

2.2. Synthesis of Ag/AgX/BiOX. Ag/AgX/BiOX (X = Cl, Br) was synthesized as follows: 0.82 g of $Bi(NO_3)_3{\cdot}5H_2O$ and 0.024 g of $AgNO_3$ were dissolved in 50 mL of deionized water (pH = 3). Then 50 mL of CTAX (X = Cl, Br, 8×10^{-3} mol/L) solution was dropped into a $Bi(NO_3)_3{\cdot}5H_2O$ and $AgNO_3$ solution. The mixture was stirred and heated in a water bath at 80 °C for 3 h. After completion of the reaction, the suspension was filtered. The precipitate was washed using absolute ethanol and deionized water three times and transferred to an oven to dry at 80 °C for 24 h. For comparison, BiOX and Ag/AgX were synthesized using similar processes without adding $AgNO_3$ and $Bi(NO_3)_3{\cdot}5H_2O$, respectively.

2.3. Characterization. X-ray diffraction patterns (XRD) of the samples was recorded at room temperature with a Bruker D8 advance X-ray diffractometer using Cu Kα radiation and a 2θ scan rate of 6 min^{-1}. Diffraction patterns were taken over the 2θ range 20−70°. X-ray photoelectron spectroscopy (XPS) measurements were carried out by a VG Multilab 2000 spectrometer (Thermo Electron Corporation) with a Mg Kα X-ray source, and the spectra were calibrated to the C 1s peak at 284.6 eV. Field emission scanning electron microscope (FESEM) images were obtained by a JEOL JEM-6700F field emission scanning electron microscope operating at an accelerating voltage and applied current of 15 kV and 10 mA, respectively. Transmission electron microscopy (TEM) and HRTEM images were obtained with a JEOL JEM-2000 (RH) field emission electron microscope operating at an accelerating voltage of 200 kV. UV−vis diffuse reflectance spectra (DRS) were obtained using a Shimadzu UV-3600 spectrometer with $BaSO_4$ as a reference.

2.4. Photocatalytic Activity Test. The photocatalytic activities were evaluated by the degradation of RhB under visible light ($\lambda \geq 400$ nm) irradiation. The visible light was obtained by a 500 W, high-pressure xenon lamp with a 400 nm cutoff filter to ensure the needed irradiation light. The xenon lamp was bought from Changzhou Yuyu Electro-Optical Device Co., Ltd. China. A typical photocatalytic degradation process is arranged in this way: 50 mL of aqueous suspension of 10 mg/L RhB was placed in a quartz glass beaker, and then 10 mg of photocatalysts was added. Prior to irradiation, the suspension was sonicated for 10 min and then magnetically stirred in the dark for 30 min to reach desorption−adsorption equilibrium. The suspension was kept under constant air-equilibrated conditions during irradiation. A magnetic stirrer was employed for continuous mixing. At certain time intervals, 4 mL suspensions were sampled and centrifuged using a TGL-16G centrifuge (Shanghai Anting Scientific Instrument Factory, China) at 10 000 rpm for 15 min to remove the particles. The upper clear liquid was analyzed by recording the maximum absorption band (553 nm for RhB) and UV−visible spectra using a Shimadzu UV-3600 spectrophotometer.

2.5. Active Species Trapping and Superoxide Radical Quantification Experiments. For detecting the active species during photocatalytic reactivity, hydroxyl radicals (·OH), the superoxide radical ($O_2^{\bullet-}$), and holes (h^+) were investigated by adding 1.0 mM IPA (a quencher of ·OH),[23−25] BQ (a quencher of $O_2^{\bullet-}$),[26,27] and TEOA (a quencher of h^+),[22,28] respectively. The method was similar to the former photocatalytic activity test. NBT (2.5×10^{-5} mol/L, exhibiting an absorption maximum at 259 nm) was used to determine the amount of $O_2^{\bullet-}$ generating from the BiOX, Ag/AgX, and Ag/AgX/BiOX photocatalytic system. The production of $O_2^{\bullet-}$ was quantitatively analyzed by detecting the concentration of NBT with the Shimadzu UV-3600 spectrophotometer. The method was similar to the former photocatalytic activity test, with NBT replacing the RhB.

3. RESULTS AND DISCUSSION

3.1. Catalyst Characterization. The phase structure of as-prepared nanocomposite Ag/AgX/BiOX was analyzed by the XRD technique (Figure 1). For X = Cl, all of the diffraction

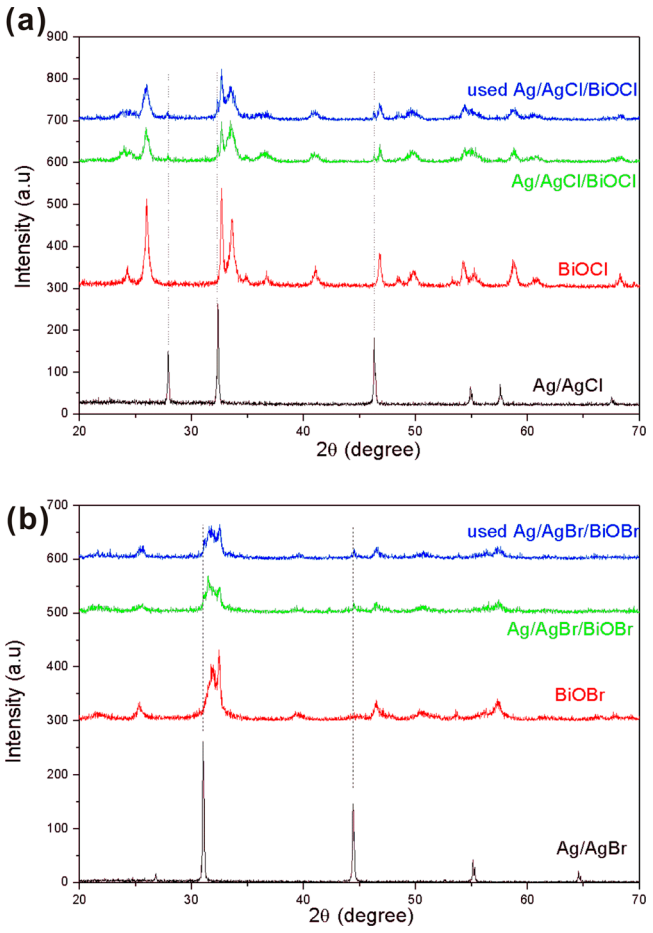

Figure 1. XRD patterns of Ag/AgX, BiOX, Ag/AgX/BiOX samples and used Ag/AgX/BiOX samples: (a) X = Cl and (b) X = Br.

peaks in the XRD patterns coincide with the standard JCPDS file no. 01-73-2060 of BiOCl and no. 85-1355 of BiOCl. For X = Br, all of the diffraction peaks in the XRD patterns coincide with the standard JCPDS file no. 01-73-2061 of BiOBr and no. 85-1356 of AgBr. However, it is difficult to prove the existence of metallic Ag according to the XRD patterns of Ag/AgX/BiOX. This phenomenon is similar to the case of Ag/AgBr/TiO_2 and Ag/AgBr/WO_3 nanocomposites.[4,16] The XRD patterns of Ag/AgX/BiOX after the PCD of RhB are also measured. It can be found that the used Ag/AgX/BiOX exhibits XRD patterns that are similar to the fresh Ag/AgX/BiOX, which indicates the Ag/AgX/BiOX is quite stable.

Figure 2 shows the surface chemical states of the Ag/AgX/BiOX with further investigation by XPS. The peak positions in

dx.doi.org/10.1021/cs300213m | ACS Catal. 2012, 2, 1677−1683

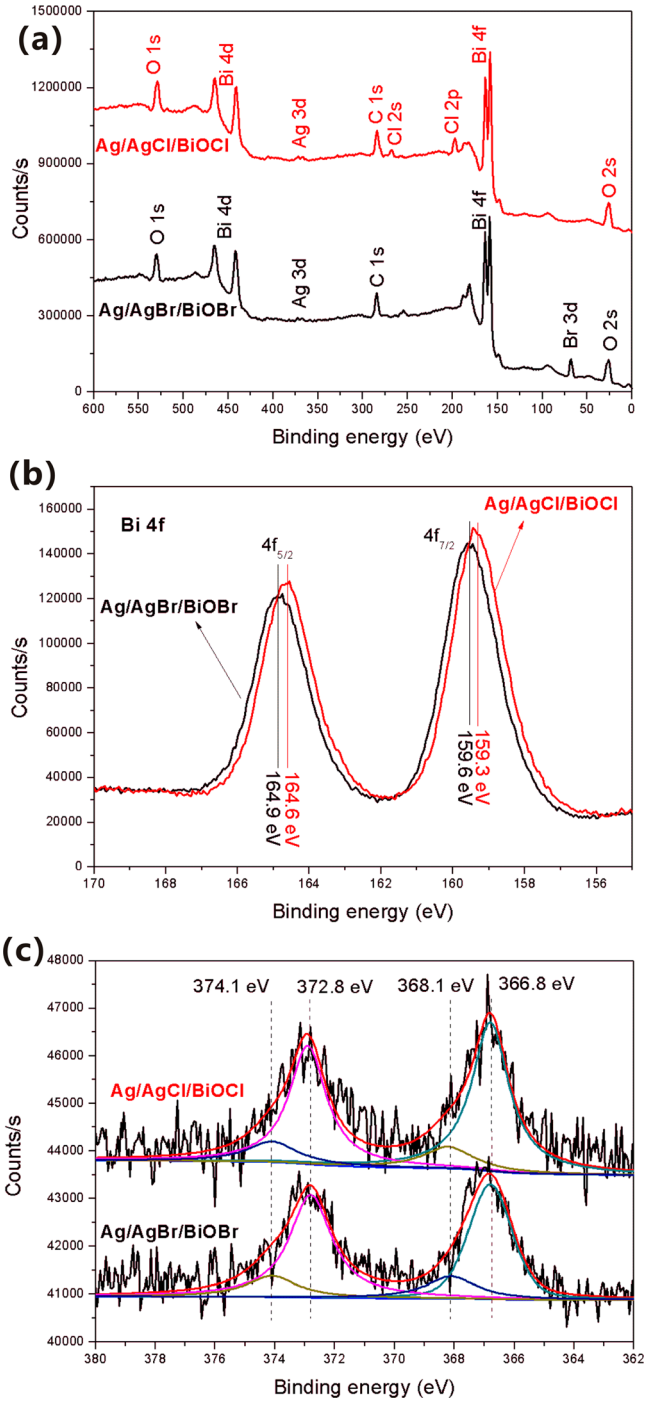

Figure 2. XPS spectra of the sample of Ag/AgX/BiOX: (a) survey XPS spectrum, (b) high-resolution XPS spectra of Bi 4f, and (c) high-resolution XPS spectra of Ag 3d.

all of the XPS spectra were calibrated with C 1s at 284.6 eV. The survey XPS spectrum of the Ag/AgX/BiOX indicates that the product consists of Ag, Bi, O, and X elements (Figure 2a). For X = Cl, two strong peaks at 159.3 and 164.6 eV shown in Figure 2b are attributed to Bi $4f_{7/2}$ and Bi $4f_{5/2}$, respectively, which are characteristic of Bi^{3+} in Ag/AgCl/BiOCl.[20,22,29] For X = Br, two strong peaks at 159.6 and 164.9 eV shown in Figure 2b are attributed to Bi $4f_{7/2}$ and Bi $4f_{5/2}$, respectively, which are characteristic of Bi^{3+} in Ag/AgBr/BiOBr.[30] Typical peaks of Ag 3d of Ag/AgX/BiOX can be further divided into two different peaks. The peaks at 366.8 and 372.8 eV are attributed to Ag(I) of AgX, and the peaks at 368.1 and 374.1 eV are attributed to metallic Ag(0) (Figure 2c). This result is in agreement with previous reports.[5,9,29,30] On the base of XPS results, it can confirm the coexistence of Ag(0) and AgX on the surface of BiOX.

On the other hand, on the basis of the XPS analysis, the surface contents of Ag(0) and Ag(I) on the surface of Ag/AgCl/BiOCl are calculated to be 0.82 and 2.93 mol %, respectively, and Ag(0) and Ag(I) on the surface of Ag/AgBr/BiOBr are calculated to be 1.13 and 2.25 mol %, respectively. This means that the surface of BiOX is not completely covered by metallic Ag and AgX species.

To further obtain the morphology and structure information, the FESEM, TEM, and HRTEM analysis of the Ag/AgX/BiOX nanocomposites have been applied (Figure 3). FESEM and

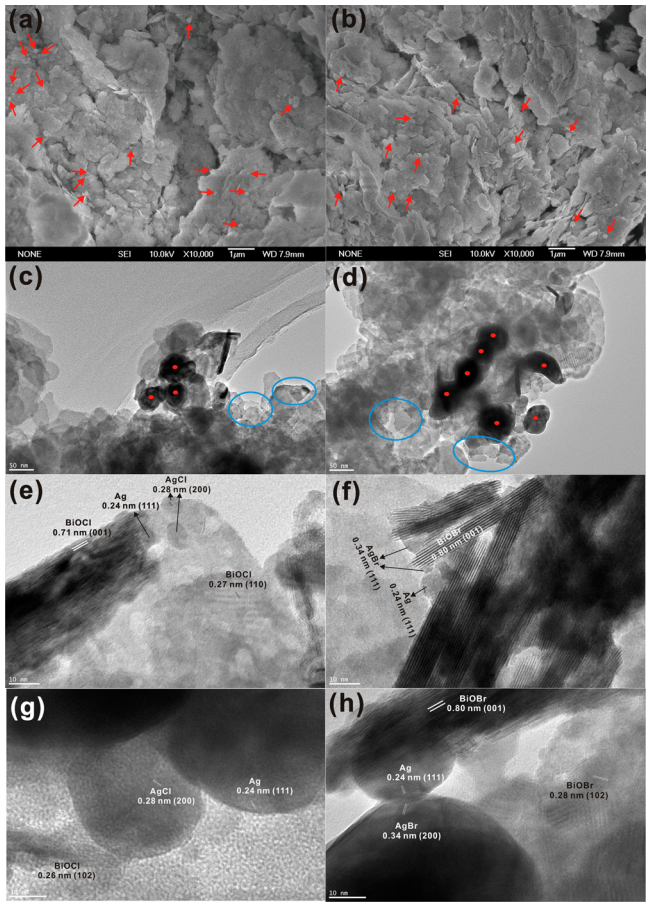

Figure 3. FESEM images of Ag/AgCl/BiOCl (a) and Ag/AgBr/BiOBr (b): the red arrows pointing out the Ag/AgX. TEM images of Ag/AgCl/BiOCl (c) and Ag/AgBr/BiOBr (d): blue rings show the small Ag/AgX, and the red dots point out the large Ag/AgX. HRTEM images of Ag/AgCl/BiOCl (e) and Ag/AgBr/BiOBr (f) with small Ag/AgX and HRTEM images of Ag/AgCl/BiOCl (g) and Ag/AgBr/BiOBr (h) with large Ag/AgX.

TEM images (Figure 3a–d) of Ag/AgX/BiOX display that Ag/AgX nanoparticles have two uniform sizes: small (5–10 nm) and large (~50–100 nm). For X = Cl, HRTEM images of Ag/AgCl/BiOCl with small (Figure 3e) and large Ag/AgCl (Figure 3g) show that the distinct lattice fringes of d = 0.71, 0.27, 0.26, 0.28, and 0.24 nm match with the crystallographic planes of BiOCl(001), BiOCl(110), BiOCl(102), AgCl(200), and Ag(111), respectively. For X = Br, Figure 3f (small size Ag/

dx.doi.org/10.1021/cs300213m | ACS Catal. 2012, 2, 1677–1683

AgBr) and h (large size Ag/AgBr) reveal the obvious lattice fringes of d = 0.80, 0.28, 0.34, and 0.24 nm match with the crystallographic planes of anatase BiOBr(001), BiOBr(102), AgBr(200), and Ag(111), respectively (Figure 3d). All of the results further confirm the coexistence of metallic Ag and AgX in the surface of BiOX nanosheets, which is in agreement with the XPS results. The FESEM images of Ag/AgX were shown in Supporting Information Figure S1. It can be seen that AgX consisted of a large sphere (~1 um), and the smooth surfaces were covered with Ag nanograins 40 nm in size.

UV−vis diffuse reflectance spectra of BiOX and Ag/AgX/BiOX are shown in Figure 4. It is clear to see that the loading of

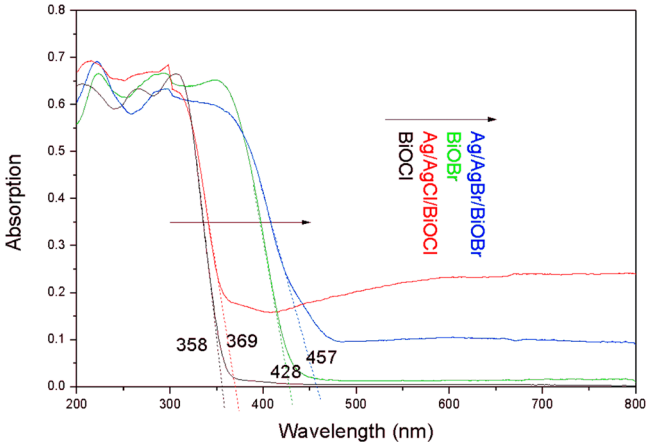

Figure 4. DRS spectra of BiOX and Ag/AgX/BiOX.

Ag/AgX onto the surface of BiOX nanosheets affects the optical property of BiOX significantly. For X = Cl, BiOCl has almost no absorbance in the visible light range, with an absorbance edge at 358 nm, and the color is white. The loading of Ag/AgCl leads to the continuous absorption band in the range of 370−800 nm, and the color is black, which results from the surface plasmon absorption of Ag nanoparticles. Furthermore, the absorbance edge increases to 369 nm. For X = Br, BiOBr has almost no absorbance, with λ > 430 nm and an absorbance edge at 428 nm. The loading of Ag/AgBr leads to the continuous absorption band in the range of 430−800 nm, and the absorbance edge increases to 457 nm, which also results from the surface plasmon absorption of metallic Ag nanoparticles;[4,12] however, the DRS spectrum of Ag/AgX/BiOX does not show a sharper peak between 400 and 500 nm depending on the surrounding dielectric properties. That is because of the inhomogeneous size of the metallic Ag particles, as shown in Figure 3.

3.2. Photocatalytic Activity. RhB is one kind of organic azo dye that is often used as a model pollutant to study the catalytic performance of photocatalysts. In this study, RhB was chosen as the target pollutant to trace the photocatalytic activity of Ag/AgX/BiOX under visible-light irradiation. The PCD experiments of RhB by Ag/AgX, BiOX, and Ag/AgX/BiOX were comparatively performed (Figure 5). Under visible light irradiation, the Ag/AgX/BiOX composites show much better photocatalytic activity than Ag/AgX or BiOX alone. Figure 5b shows that the photocatalytic degradation of RhB on different catalysts fits pseudo-first-order kinetics, $\ln(C/C_0) = kt$, where C is the concentration of the RhB at time t, C_0 is the initial concentration of the RhB solution, and the slope k is the apparent reaction rate constant. The PCD constant of Ag/

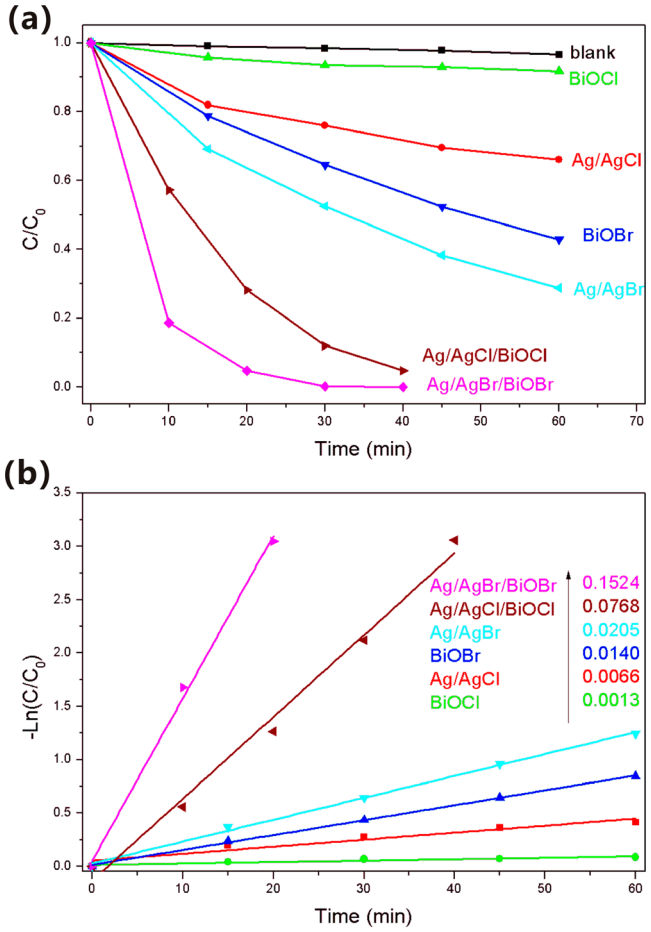

Figure 5. The PCD percentage (a) and pseudo-first-order reaction kinetics (b) of RhB under visible light irradiation ($\lambda \geq$ 400 nm).

AgCl/BiOCl (0.0768 min^{-1}) was found to be about 59 times that of BiOCl (0.0013 min^{-1}) and 12 times that of Ag/AgCl (0.0066 min^{-1}). The PCD constant of Ag/AgBr/BiOBr (0.1524 min^{-1}) was found to be about 11 times that of BiOBr (0.0140 min^{-1}) and 7 times that of Ag/AgBr (0.0205 min^{-1}).

On the basis of characterization and photocatalytic data, it can be concluded that Ag/AgX enhanced the photocatalytic activity of Ag/AgX/BiOX. However, how did the metallic Ag enhance the photocatalytic activity of Ag/AgX/BiOX? Is the role of metallic Ag the same for Ag/AgCl/BiOCl and Ag/AgBr/BiOBr? To answer these questions, the photogenerated active species in Ag/AgCl/BiOCl and Ag/AgBr/BiOBr were investigated.

3.3. Photocatalytic Mechanism of Ag/AgCl/BiOCl: Surface Plasmon Resonance. Figure 6a displays the trapping experiment of active species during the photocatalytic reaction. It can be seen that the photocatalytic degradation of RhB was not affected by the addition of 1 mM IPA (a quencher of ·OH) and BQ (a quencher of $O_2^{\bullet-}$). On the contrary, the photocatalytic degradation of RhB obviously decreased with the addition TEOA (a quencher of h^+). Therefore, it can be concluded that holes are the main active species of Ag/AgCl/BiOCl in aqueous solution under visible light irradiation, rather than $O_2^{\bullet-}$ or ·OH. In addition, a colorless molecular probe, nitroblue tetrazolium (NBT) was chosen to quantify the $O_2^{\bullet-}$ concentration of BiOCl, Ag/AgCl, and Ag/AgCl/BiOCl. It was found that the generation of $O_2^{\bullet-}$ decreased after the Ag/AgCl

dx.doi.org/10.1021/cs300213m | ACS Catal. 2012, 2, 1677−1683

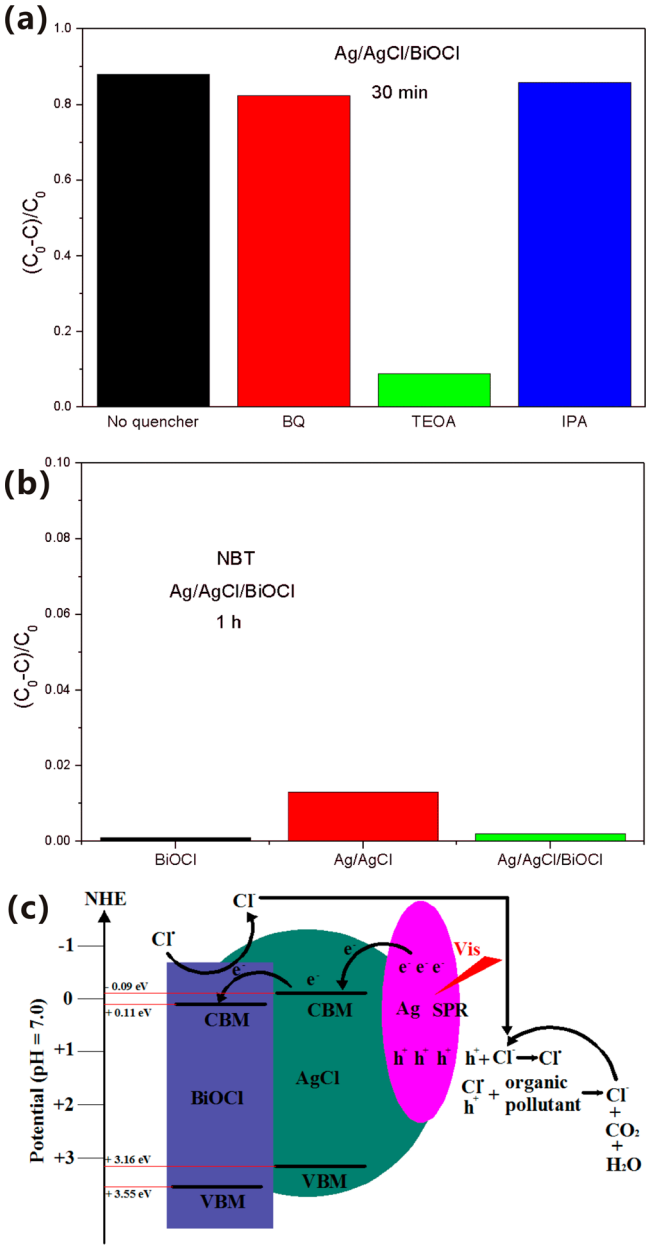

Figure 6. Photocatalytic mechanism for Ag/AgCl/BiOCl: (a) trapping experiment of active species during the photocatalytic reaction; (b) transformation percentage of NBT concentration by Ag/AgCl, BiOCl, and Ag/AgCl/BiOCl; and (c) photocatalytic mechanism scheme of Ag/AgCl/BiOCl under visible light irradiation ($\lambda \geq 400$ nm).

coupling on BiOCl nanosheets (Figure 6b). It is in agreement with the result of the trapping experiment.

To explain the enhanced photocatalytic activity mechanism, conduction band minimum (CBM) and valence band maximum (VBM) potentials of AgX and BiOX should be confirmed. For a semiconductor, the CBM and VBM can be calculated according to an empirical equation: $E_{CBM} = \chi - E_e - 0.5E_g$,[17] where E_{CBM} is the CBM edge potential; χ is the electronegativity of the semiconductor, which is the geometric mean of the electronegativity of the constituent atoms; E_e is the energy of free electrons on the hydrogen scale (about 4.5 eV); E_g is the band gap energy of the semiconductor; and E_{VBM} can be determined by $E_{VBM} = E_{CBM} + E_g$. The values used for calculating the CBM and VBM potentials of BiOX and AgX are listed in Table 1.

Table 1. Calculation of the CB and VB Potentials of AgX and BiOX

	χ	E_g, eV	E_{CB}, eV	E_{VB}, eV
AgCl	6.04	3.25	−0.09	3.16
BiOCl	6.33	3.44	0.11	3.55
AgBr	5.81	2.60	−0.30	2.30
BiOBr	6.17	2.90	0.22	3.12

The photocatalytic mechanism scheme of Ag/AgCl/BiOCl photocatalyst is shown in Figure 6c. It can be found that BiOCl and AgCl cannot be excited by visible light. Thanks to the SPR and dipolar character of metallic Ag, metallic Ag can absorb visible light, and the absorbed photon would be efficiently separated to an electron and a hole.[12] Then electrons transfer to the CBM of AgCl and further transfer to the CB of BiOCl. This electron transfer process can decrease the recombination of charges. However, it is a pity that the electrons on the CBM of BiOCl cannot react with O_2 to produce $O_2^{\bullet-}$ for the CBM potential of BiOCl (0.11 eV vs NHE) is more positive than $E_0(O_2/O_2^{\bullet-})$ (−0.046 eV vs NHE),[1] so the generation of $O_2^{\bullet-}$ decreased after the Ag/AgCl coupling on BiOCl nanosheets (Figure 6b). However, the photogenerated holes transfer to the AgCl and BiOCl surface, which corresponds to the oxidation of Cl^- ions to Cl· radicals.[28,29] The Cl· radical is a reactive radical species that can oxidize RhB, and hence, Cl· is reduced to Cl^- ions again. Of course, photogenerated electrons at the CBM of BiOCl also can reduce Cl· to Cl^- ions,[28,31] so the Ag/AgCl/BiOCl photocatalyst displays enhanced photocatalytic activity. On the base of above photocatalytic mechanism discussion, it can be suggested that metallic Ag plays a very important role in SPR. Of course, a double Cl^- ions source from AgCl and BiOCl may be another factor to improve the photocatalytic activity.

3.4. Photocatalytic Mechanism of Ag/AgBr/BiOBr: Z-Scheme Bridge. Ag/AgBr/BiOBr and Ag/AgCl/BiOCl are the same series three-component VLD photocatalysts. Does the metallic Ag play the same role?

Figure 7a displays the trapping experiment of active species during the photocatalytic reaction of Ag/AgBr/BiOBr. It can be found that the photocatalytic degradation of RhB was not affected by the addition of 1 mM IPA. On the contrary, the photocatalytic degradation of RhB obviously decreased with the addition of TEOA and BQ. Therefore, it can be concluded that h^+ and $O_2^{\bullet-}$ are the main active species of Ag/AgBr/BiOBr in aqueous solution under visible light irradiation. Figure 7b displays the transformation percentage of NBT. For BiOBr, the transformation percentage of NBT can be neglected. It is due to the CBM potential of BiOBr (0.22 eV vs NHE) being more positive than $E_0(O_2/O_2^{\bullet-})$ (−0.046 eV vs NHE);[1] however, Ag/AgBr and Ag/AgBr/BiOBr show transformation percentages for NBT of 5.5% and 9.3%, respectively, so the photocatalytic activity of Ag/AgBr/BiOBr was obviously affected by BQ (Figure 7a). This result is different from that of Ag/AgCl/BiOCl. Therefore, the photocatalytic mechanism and the role of metallic Ag may be different from that of Ag/AgCl/BiOCl.

At first, if the metallic Ag plays a SPR role, the photoinduced electrons are transferred to the CBM of BiOBr for the more positive CBM potential of BiOBr, and there is no $O_2^{\bullet-}$ production, but the transformation of NBT and trapping

dx.doi.org/10.1021/cs300213m | ACS Catal. 2012, 2, 1677−1683

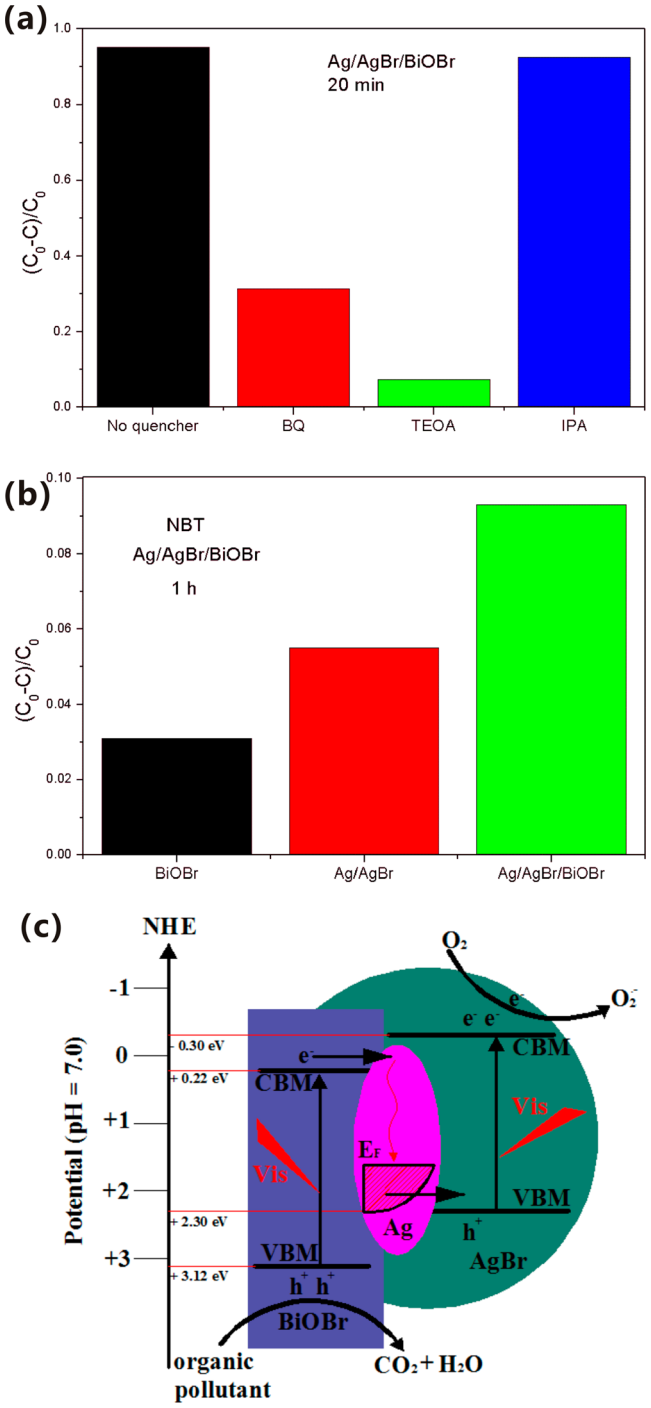

Figure 7. Photocatalytic mechanism for Ag/AgBr/BiOBr: (a) trapping experiment of the active species during the photocatalytic reaction, (b) transformation percentage of NBT concentration by Ag/AgBr, BiOBr and Ag/AgBr/BiOBr, and (c) photocatalytic mechanism scheme of Ag/AgBr/BiOBr under visible light irradiation ($\lambda \geq 400$ nm).

experiment proved the enhancement of the generation of $O_2^{\bullet-}$, so the main role of metallic Ag is not SPR in Ag/AgBr/BiOBr. Considering AgBr and BiOBr can absorb visible light and be excited, which is different from AgCl and BiOCl, the possible role maybe is the Z-scheme bridge, which also has been proved in Au/CdS/TiO_2,[32] Ag/AgBr/Bi_2WO_6,[4] and Ag/AgBr/TiO_2 systems.[13]

Figure 7c shows the possible photocatalytic mechanism scheme of the Ag/AgBr/BiOBr photocatalyst. Under visible light irradiation, both AgBr and BiOBr are excited, and the photogenerated holes and electrons are in their VBM and CBM, respectively. On one hand, CBM electrons of BiOBr easily flow into metal Ag (electron transfer I: $BiOBr_{CBM} \rightarrow Ag$) through the Schottky barrier because the CB potential of BiOBr is more negative than that Fermi level of the loaded metal Ag. On the other hand, since the Fermi level of Ag is more positive than the VBM of AgBr, VBM holes of AgBr also easily flow into metal Ag (electron transfer II: $Ag \rightarrow AgBr_{VBM}$), which is faster than the electron−hole recombination between the VBM and CBM of AgBr.[4,32] Therefore, simultaneous electron transfers I and II ($BiOBr_{CBM} \rightarrow Ag \rightarrow AgBr_{VBM}$) enhance separation of VBM holes (BiOBr) and CBM electrons (AgBr). Therefore, the Ag/AgBr/BiOBr photocatalyst shows improved photocatalytic activity.

4. CONCLUSIONS

In this paper, Ag/AgX/BiOX (X = Cl, Br) was synthesized by a facile deposition−precipitation method. On the basis of their efficient photocatalytic activity, the three-component VLD photocatalysts could be widely used for environmental purification of organic pollutants in aqueous solution. In addition, the role of metallic Ag in Ag/AgCl/BiOCl and Ag/AgBr/BiOBr were analyzed, and we found that the role of metallic Ag was SPR and the Z-scheme bridge for Ag/AgCl/BiOCl and Ag/AgBr/BiOBr, respectively. It indicates that metallic Ag can enhance VLD photocatalytic activity not only for narrow band gap photocatalysts ($E_g < 3.1$ eV) but also for wide band gap photocatalysts ($E_g > 3.1$ eV) though the different roles.

■ ASSOCIATED CONTENT

Supporting Information

Additional FESEM images of AgCl and AgBr. This material is available free of charge via the Internet at http://pubs.acs.org.

■ AUTHOR INFORMATION

Corresponding Author

*Phone: 86 27 6875 2919. Fax: 86 27 8737 8727. E-mail: irlab@whu.edu.cn.

Notes

The authors declare no competing financial interest.

■ ACKNOWLEDGMENTS

This work was supported by National Natural Science Foundation of China (No: 20973128) and open foundation of key laboratory of catalysis and materials science of the state ethnic affairs commission and ministry of education, south-central university for nationalities. The authors acknowledge the assistance from Center for Electron Microscopy, Wuhan University.

■ REFERENCES

(1) Chen, C.; Ma, W.; Zhao, J. *Chem. Soc. Rev.* **2010**, *39*, 4206−4219.
(2) Linsebigler, A. L.; Lu, G.; Yates, J. T. *Chem. Rev.* **1995**, *95*, 735−758.
(3) Zhang, L.; Wong, K. H.; Chen, Z.; Yu, J. C.; Zhao, J.; Hu, C.; Chan, C. Y.; Wong, P. K. *Appl. Catal., A* **2009**, *363*, 221−229.
(4) Zhang, Y.; Tang, Z. R.; Fu, X.; Xu, Y. J. *Appl. Catal., B* **2011**, *106*, 445−452.
(5) Wang, P.; Huang, B.; Qin, X.; Zhang, X.; Dai, Y.; Wei, J.; Whangbo, M. H. *Angew. Chem., Int. Ed.* **2008**, *47*, 7931−7933.

(6) Wang, P.; Huang, B.; Lou, Z.; Zhang, X.; Qin, X.; Dai, Y.; Zheng, Z.; Wang, X. *Chem.—Eur. J.* **2010**, *16*, 538−544.
(7) Wang, P.; Huang, B.; Zhang, X.; Qin, X.; Jin, H.; Dai, Y.; Wang, Z.; Wei, J.; Zhan, J.; Wang, S.; Wang, J.; Whangbo, M. H. *Chem.—Eur. J.* **2009**, *15*, 1821−1824.
(8) An, C.; Peng, S.; Sun, Y. *Adv. Mater.* **2010**, *22*, 2570−2574.
(9) Zhu, M.; Chen, P.; Liu, M. *ACS Nano* **2011**, *5*, 4529−4536.
(10) Xu, H.; Li, H.; Xia, J.; Yin, S.; Luo, Z.; Liu, L.; Xu, L. *ACS Appl. Mater. Interfaces* **2011**, *3*, 22−29.
(11) Li, Y.; Ding, Y. *J. Phys. Chem. C* **2010**, *114*, 3175−3179.
(12) Linic, S.; Christopher, P.; Ingram, D. B. *Nature Mater.* **2011**, *10*, 911−921.
(13) Tian, G.; Chen, Y.; Bao, H. L; Meng, X.; Pan, K.; Zhou, W.; Tian, C.; Wang, J. Q.; Fu, H. *J. Mater. Chem.* **2012**, DOI: 10.1039/c1jm13820k.
(14) Elahifard, M. R.; Rahimnejad, S.; Haghighi, S.; Gholami, M. R. *J. Am. Chem. Soc.* **2007**, *129*, 9552−9553.
(15) Zhang, L. S.; Wong, K. H.; Yip, H. Y.; Hu, C.; Yu, J. C.; Chan, C. Y.; Wong, P. K. *Environ. Sci. Technol.* **2010**, *44*, 1392−1398.
(16) Wang, P.; Huang, B.; Qin, X.; Zhang, X.; Dai, Y.; Whangbo, M. H. *Inorg. Chem.* **2009**, *48*, 10697−10702.
(17) Zhang, X.; Ai, Z.; Jia, F.; Zhang, L. *J. Phys. Chem. C* **2008**, *112*, 747−753.
(18) Zhang, K. L.; Liu, C. M.; Huang, F. Q.; Zheng, C.; Wang, W. D. *Appl. Catal., B* **2006**, *68*, 125−129.
(19) Cheng, H.; Huang, B.; Wang, Z.; Qin, X.; Zhang, X.; Dai, Y. *Chem.—Eur. J.* **2011**, *17*, 8039−8043.
(20) Ye, L.; Zan, L.; Tian, L.; Peng, T.; Zhang, J. *Chem. Commun.* **2011**, *47*, 6951−6953.
(21) Ye, L.; Tian, L.; Peng, T.; Zan, L. *J. Mater. Chem.* **2011**, *21*, 12479−12484.
(22) Ye, L; Deng, K.; Xu, F.; Tian, L.; Peng, T.; Zan, L. *Phys. Chem. Chem. Phys.* **2012**, *14*, 82−85.
(23) Ji, P.; Zhang, J.; Chen, F.; Anpo, M. *Appl. Catal., B* **2009**, *85*, 148−154.
(24) Bowmaker, G. A.; Skelton, B. W.; White, A. H. *Inorg. Chem.* **2009**, *48*, 3185−3197.
(25) Zhou, L.; Liu, J.; Liu, Z. *J. Hazard. Mater.* **2009**, *172*, 439−446.
(26) Khan, S. A.; Singh, N.; Saleem, K. *Eur. J. Med. Chem.* **2008**, *43*, 2272−2277.
(27) Bolzana, A. E.; Iwasita, T.; Arvia, A. J. *J. Electroanal. Chem.* **2003**, *55*, 49−60.
(28) Chen, F.; Liu, H.; Bagwasi, S.; Shen, X.; Zhang, J. *J. Photochem. Photobiol. A* **2010**, *215*, 76−80.
(29) Jiang, J.; Zhang, L. *Chem.—Eur. J.* **2011**, *17*, 3710−3717.
(30) Cheng, H.; Huang, B.; Wang, P.; Wang, Z.; Lou, Z.; Wang, J.; Qin, X.; Zhang, X.; Dai, Y. *Chem. Commun.* **2011**, *47*, 7054−7056.
(31) Gondal, M. A.; Chang, X. F.; Yamani, Z. H. *Chem. Eng. J.* **2010**, *165*, 250−257.
(32) Tada, H.; Mitsu, T.; Kiyonaga, T.; Akita, T.; Tanaka, K. *Nat. Mater.* **2006**, *5*, 1−5.